Analysis of Flow Structures in Wake Flows for Train Aerodynamics

by

Tomas W. Muld

May 2010
Technical Reports
Royal Institute of Technology
Department of Mechanics
SE-100 44 Stockholm, Sweden

Akademisk avhandling som med tillstånd av Kungliga Tekniska Högskolan i Stockholm framlägges till offentlig granskning för avläggande av teknologie licentiatsexamen fredagen den 28 maj 2010 kl 13.15 i sal MWL74, Kungliga Tekniska Högskolan, Teknikringen 8, Stockholm.

Universitetsservice US–AB, Stockholm 2010

Till Mamma ♡

The Only Easy Day Was Yesterday

Motto of the United States Navy SEALs

Aerodynamics are for people who can't build engines

Enzo Ferrari

Analysis of Flow Structures in Wake Flows for Train Aerodynamics

Tomas W. Muld
Linné Flow Centre, KTH Mechanics, Royal Institute of Technology
SE-100 44 Stockholm, Sweden

Abstract

Train transportation is a vital part of the transportation system of today and due to its safe and environmental friendly concept it will be even more important in the future. The speeds of trains have increased continuously and with higher speeds the aerodynamic effects become even more important. One aerodynamic effect that is of vital importance for passengers' and track workers' safety is slipstream, i.e. the flow that is dragged by the train. Earlier experimental studies have found that for high-speed passenger trains the largest slipstream velocities occur in the wake. Therefore the work in this thesis is devoted to wake flows. First a test case, a surface-mounted cube, is simulated to test the analysis methodology that is later applied to a train geometry, the Aerodynamic Train Model (ATM). Results on both geometries are compared with other studies, which are either numerical or experimental. The comparison for the cube between simulated results and other studies is satisfactory, while due to a trip wire in the experiment the results for the ATM do not match. The computed flow fields are used to compute the POD and Koopman modes. For the cube this is done in two regions of the flow, one to compare with a prior published study Manhart & Wengle (1993) and another covering more of the flow and especially the wake of the cube. For the ATM, a region containing the important flow structures is identified in the wake, by looking at instantaneous and fluctuating velocities. To ensure converged POD modes two methods to investigate the convergence are proposed, tested and applied. Analysis of the modes enables the identification of the important flow structures. The flow topologies of the two geometries are very different and the flow structures are also different, but the same methodology can be applied in both cases. For the surface-mounted cube, three groups of flow structures are found. First group is the mean flow and then two kinds of perturbations around the mean flow. The first perturbation is at the edge of the wake, relating to the shear layer between the free stream and the disturbed flow. The second perturbation is inside the wake and is the convection of vortices. These groups would then be typical of the separation bubble that exists in the wake of the cube. For the ATM the main flow topology consists of two counter rotating vortices. This can be seen in the decomposed modes, which, except for the mean flow, almost only contain flow structures relating to these vortices.

Descriptors: Train Aerodynamics, Slipstream, Wake Flow, Detached-Eddy Simulation, Proper Orthogonal Decomposition, Koopman Mode Decomposition, Surface-mounted Cube, Aerodynamic Train Model

Preface

The second part is a collection of the following articles:

Paper 1. T.W. Muld, G. Efraimsson and D.S. Henningson,
Mode Decomposition on a Surface-Mounted Cube
Submitted to Flow, Turbulence and Combustion (2010)

Paper 2. T.W. Muld, G. Efraimsson, D.S. Henningson, A.H. Herbst and A. Orellano,
Detached Eddy Simulation and Validation on the Aerodynamic Train Model
Proceedings of EUROMECH COLLOQUIUM 509: Vehicle Aerodynamics (2009)

Paper 3. T.W. Muld, G. Efraimsson and D.S. Henningson,
Mode Decomposition of the Flow Behind the Aerodynamic Train Model Simulated by Detached Eddy Simulation
Internal report (2010), TRITA-AVE 2010:28, ISSN 1651-7660

Division of work between authors
The work is done within the research program *Gröna Tåget*, which is financed by *Banverket* (Swedish Rail Administration). The title of the project is **Front shape and slipstream for wide body trains at higher speeds** and is a collaboration between KTH and Bombardier Transportation. The work has been supervised by Prof. Dan S. Henningson(DH) and Dr. Gunilla Efraimsson(GE) at KTH. Leading the research project is Dr. Astrid H. Herbst (AH) from Bombardier Transportation, also involved in the project is Dr. Alexander Orellano(AO), also from Bombardier Transportation.

Paper 1
Simulations, post-processing, mode decomposition, analysis and writing of the paper were performed by TM. The work and paper were reviewed by GE and DH.

Paper 2
Simulations, post-processing, analysis and writing of the paper were performed by TM. The work and paper were reviewed by GE and DH. Original mesh, geometry and experimental data were provided by AH.

Paper 3
Simulations, post-processing, mode decomposition, analysis and writing of the paper were performed by TM. The work and paper were reviewed by GE and DH. Original mesh, geometry and experimental data were provided by AH.

Part I

Introduction

CHAPTER 1

Introduction

Trains have moved people and goods around countries and continents ever since Stephenson's *Rocket* won the Rainhill Trials in 1829; a competition where the winning design would traffic the newly built railway between Liverpool and Manchester. Eventough new transportation systems have arisen since 1829, the railways are still a vital part of the transportation in today's society. To remain competitive against air and road transport, there has been a development towards shorter travel times with high-speed trains, which is defined as trains travelling above 200 km/h. The speed of trains can increase even more in the future and as the price for oil increases, punishing petrol based transportation, trains can become even more important within the transportation sector.

Two of the strongest arguments for rail transport versus other transportation systems are the good safety and lower emission of greenhouse gases. Stephenson's Rocket was driven by steampower, but today's trains, and especially high-speed trains, are mostly powered by electrical engines. The electricity is taken from the main power grid and the amount of emissions are then decided by the way the electricity is generated nationally. This depends on country and season, and could vary from wind, hydro or nuclear power with low emission of greenhouse gases to coal power with larger emissions. The overall environmental effects of nuclear power can be discussed further, but this is out of the scope of this thesis. Other means of transportation are mainly powered by fossil fuels which have very large emissions of greenhouse gases. In Andersson & Berg (2007), the emission of carbon dioxid is compared between air, road and rail transport in Sweden during 2005. Rail transport emitted 0.1 Mton CO_2, road transport 18.5 Mton and air transport 0.6 Mton. Since rail transportation is dependant on the type of power generation on the main power grid, the only way train industry can influence the emissions is to reduce the energy consumption of the trains produced. Development of regenerative brakes and improvement of aerodynamic resistance are examples of two efforts made for accomplishing higher energy efficiency, but more can be done.

The good safety of trains originates from the fact that train transportation is conducted on a separate track isolated from other type of transport.

The safety on track is maintained by strict rules and advanced safety systems. Although strong safety consideration, accidents do happen, but in a smaller amount than for other means of transportations. In Andersson & Berg (2007) the number of people fatally injured in Sweden per every kilometer and person transported is compared between transportation systems. For air transport, buses, passenger cars and trains the amounts are 0.2-0.4, 0.2-0.3, 4 and 0.15, respectively. This statistics clearly states that trains are the safest way of transportation followed by air and buses, while passenger cars have the most fatal accidents. The difference between passenger cars and other transport systems is an order of magnitude. There are different reasons for accidents involving trains, where some of them are related to the air flow around the train. To improve the safety even further, the aerodynamic effects have to be investigated. This is especially important as trains become faster since the aerodynamic effects become more dominate at higher speeds. Hence aerodynamics is important for making high-speed trains both safe and environmental friendly.

1.1. Train Aerodynamics

Train aerodynamics covers a wide range of different topics concerned with the air flow around trains. Some of these topics are shared with road vehicles such as drag, crosswind and aeroacoustics, while others are specific to trains such as slipstream, ballast projection, tunnel exits and head pressure pulse. One of the challenges specific to train aerodynamics is the long slender body of a train causing a large boundary layer at the rear. A few of the topics in train aerodynamics are presented below.

Crosswind is of importance when the wind component perpendicular to the track is large, which could cause problem of stability of the vehicle, for trains see e.g. Hamida *et al.* (2005) and Diedrichs (2009). One special case of crosswind that could be extra difficult is when the vehicle move into unsteady wind gusts, see Favre (2009) for a car shaped vehicle. Another case of interest for crosswind is when a train exits a tunnel with large wind velocities outside the tunnel. Since only part of the train is exposed to the crosswind a large yawing moment is created, see Bocciolone *et al.* (2008). Ballast projection deals with the flow under the train and through the bogies. This phomenon is simulate in order to predict the motion of the objects located underneath the train in the ballast. When the train passes it creates aerodynamic load on the object, which, if strong enough, could lift the object. This is a problem for the equipment underneath the train that could be hit by a flying object. Further information on ballast projection can be found in Jönsson *et al.* (2009).

When designing a high-speed train, all aerodynamic aspects have to be considered. Creating an optimal shape may prove to be a difficult task since an optimized shape for one flow phenomenon may not be optimal for another,

for some phenomenon it might actually be far from an optimal shape. This requires some compromise in order to find an aerodynamic shape that fulfill all the requirements. Other requirements on the shape are for instance concerned with crash zones and the driver's visibility of the track. One requirement that is not demanded by other types of vehicles is that the front should have the same shape as the rear. This is because both sides are used as front and rear depending which direction the train is moving. The limited space and time at end station makes it impossible to turn train sets, yielding the solution of moving the train in both direction instead. However, the disadvantage of this solution is that the train needs to be symmetric, and what is an optimal shape for the front does not necessary provide a good flow field at the rear of the train.

This thesis addresses the aerodynamic topic of slipstream. Slipstream is the air that is dragged with the train, due to the viscosity of the fluid. This phenomenon can for instance be felt by passengers standing on platforms. As the train passes and even for a time after it has passed a person standing on a platform can experience wind gusts originating from the train. This is a safety concern for passengers standing on platforms, trackside workers, pushchair and bagage on platforms. If the slipstream velocities are too strong it could knock a person of her (or his) feet or move objects located close to the train. The Rail Safety & Standards board in the United Kingdom (UK), Figura-Hardy (2007), summarized incidents in the UK between 1972 and 2005 that could be related to slipstream. Four incidents with passengers or staff on platforms, two with trackside workers and 13 involving pushchairs were found during this period. One case involved a child located in the pushchair that substained minor head injury.

The regulation that sets the standard for slipstream is the Technical Specifications for Interoperability (TSI). This is a set of standards formulated by the European Railway Agency (ERA) for the Trans-European Rail network lines and decided upon by the European Commission. The purpose is to standardize the requirements and enable trains from different European countries to operate on the same track. The TSI states that a train operating at 200 km/h should not cause slipstream velocities higher than 15.5 m/s at 1.2 m above the platform at a distance 3.0 m from the center of the track. There is also a corresponding standard for slipstream running on open track, which states that a train running at 190-249 km/h should not cause velocities exceeding 20.0 m/s at 0.2 m above top of rail (TOR) and 3.0 m from the center of the track, Barrot (2008). Both these regulations are defined at a distance from the center of the track and do not consider the width of the train. In Sweden there are other regulations on the width of trains than in central Europe. This enables wider train concepts, such as the Regina from Bombardier Transportation, see Figure 1.1. Shorter trains can be used to transport the same amount of people since the Regina can accommodate 5 sitting passengers (3+2) in every row instead of 4 (2+2).

FIGURE 1.1. The Regina train from Bombardier Transportation

However, the wide car body causes problems for slipstream since the side wall of the train comes closer to the measurement point located at a fixed distance from the centre of track and closer to the people standing on the platform.

In Sterling *et al.* (2008) slipstream is divided into four regions; head passage, boundary layer, near wake and far wake. When the head of the train passes, the flow is accelerated and decelerated around the train, causing a pressure pulse. Thereafter, the boundary layer grows when the train passes, which is the second region. The region known as the near wake comes just after the passage of the rear of the train. Depending on the shape of the train, the flow in this region could be very different. In Morel (1980) and Ahmed *et al.* (1984) two different flow topologies were found by altering the slant angle of a circular cylinder. These were a large separation bubble or two counter rotating vortices. Depending on the shape of the train the flow in the near wake would be either of these topologies. The far wake is the region long after the train has passed. The flow is still disturbed by the passing train, but not as severely as in the near wake. From the experiments summarized in Sterling *et al.* (2008) it can be seen that the largest slipstream velocities arise in different regions depending on type of train. For freight trains the largest velocities are in the boundary layer zone, while for high-speed trains the largest velocities are located in the near wake. This means that in order to understand slipstream for a high-speed train the flow behind the train in the wake have to be well simulated and a solid physical understanding of the flow structures is needed. The near wake region and the flow structures are therefore the focus of this thesis.

Research and development in train aerodynamics is either done with the help of numerical simulations or by conducting experiments. Experiments can either be performed at full scale on a real track or with scaled models put in wind tunnels or water towing tanks. Full scale tests are performed on existing tracks with measurement equipment mounted close to the track. This means that measurements can only be taken once for each train passing, which makes full scale tests very expensive. The measurement devices also have to be mounted on the side of the track, which does not give a complete flow field. In

addition the ambient conditions are impossible to control, which complicates comparison of results for different samples. Scaled models can be placed in wind tunnels where more data of the flow field can be measured. One problem with wind tunnel experiments is the simulation of the ground. If the train model is mounted stationary to the ground, the resulting flow field is not realistic since this is not the case for trains on track. There are wind tunnels that have solved this by having moving belts to simulate the motion of the ground relative to train and ambient air. Another way to solve the problem with the ground effect is to have a moving train relative to the ground. This means that the model is attached to some kind of rail system that moves the model at constant speed. This is for instance done in water towing tanks. There are also some examples where the model passes an exhaust of a wind tunnel to simulate cross-wind. The problems with these methods are similar to those for full-scale test, but it is done within a controlled environment and more runs can be done at much lower cost than for full-scale test. The option to experimental work is to use numerical methods to simulate the flow. The advantage is that the full 3-D flow field is given from the simulation and alterations to the geometry can be done at small expenses. The disadvantage is the fact that for most realistic flow cases it is computationally too demanding to resolve the smallest turbulent flow structures, imposing that some of the turbulence scales have to be modelled. For slipstream phenomenon experimental work are available, but to the knowledge of the author, very few numerical work is published.

1.2. Coherent Flow Structures

The flow behind a train contains a large variety of time and length scales, ranging from the largest eddies to the smallest dissipative scales. Resolving all these scales for a high-speed train, which is a complex geometry with high Reynolds number flow, would be too demanding for today's computers, so some kind of modelling of the turbulence has to be performed. One approach is to model all the turbulent scales with Reynolds Average Navier-Stokes (RANS) models. These are relatively fast methods but does not capture the transient turbulence. Another type of approach is the Large-eddy Simulation (LES), which resolves the largest scales and only models the smallest dissipative scales. This is then more computational demanding since it requires a large computational grid, with many cells in the boundary layer. These two approaches could be combined into hybrid LES/RANS models. One such hybrid model is Detached-Eddy Simulation (DES), which utilizes a RANS model close to wall and LES far from wall. This does not require as many cells in the boundary layer as for LES, but still resolves the large turbulent structures in separated regions.

In order to analyze the variety of scales and flow structures different methods can be applied to decompose the temporal and spatial dependence of the flow field. The modes extracted from the splitting of the flow field can then be analyzed individually instead of analyzing the full 4-D (3 space and time) turbulent flow. With different decomposition methods the modes will have

different properties and be ordered differently. In order to perform these decompositions, the solution of the flow has to be time-accurate, that is the fluctuations in time have to be resolved. The two decomposition methods used in this thesis is Proper Orthogonal Decomposition (POD) and Koopman mode decomposition. POD (also known as Karhunen-Loève Decomposition) is a well established method and has been used in many different fields including fluid mechanics Manhart & Wengle (1993), image recognition, see Turk & Pentland (1991), and chemical reacting systems, see Krischer *et al.* (1993). In POD the flow is decomposed into orthogonal modes arranged in decreasing order of energy. Koopman mode decomposition is newly adapted in fluid mechanics, but has previously been used for non-linear dynamical systems, see Mezić (2005). Here, the modes are decomposed so that they all represent an individual frequency.

CHAPTER 2

Problem Configuration

In this thesis, two different geometries have been considered in order to analyze flow structures. The purpose of the first geometry was to be a test case for the methodology consisting of DES and POD. It was essential to choose a geometry for which published results existed in order to test the methodology. The chosen test case was the surface-mounted cube, that had been studied in Manhart & Wengle (1993), Rodi *et al.* (1997) and Martinuzzi & Tropea (1993). The other geometry is the Aerodynamic Train Model (ATM), where the methodology using DES and POD is used on an applied geometry. The reason for using this geometry was that experimental data from German Aerospace Centre (DLR) from a water towing tank was available. Other studies of this geometry are presented in Schober *et al.* (2009), where results from different wind tunnels are compared.

2.1. Surface mounted Cube

The geometry of this flow case consists of a cube, with the length H, placed on the bottom of a channel with a channel height of $2H$. The computational domain extend $10H$ in the spanwise direction and $4H$ upstream and $10H$ downstream of the cube, respectively. This is larger than the domain used in Manhart & Wengle (1993), since the computational domain in Manhart & Wengle (1993) was in initial studies by the author found to be too small. Upstream of the cube the flow is considered to be fully-developed turbulent channel flow. The upstream boundary condition is placed relatively close to the cube and therefor a fully-developed profile including turbulent fluctuations has to be applied there. The cube has sharp edges, which means that the separation point is fixed at the front edge of the cube. The geometry is shown in Figure 2.1.

The characteristic velocity scale for this problem is the bulk velocity

$$U_{bulk} = \frac{1}{2HW} \int_0^{2H} \int_{-W/2}^{+W/2} U \mathrm{d}y\mathrm{d}z \approx 23.3 \text{ m/s} \tag{2.1}$$

This can be interpreted as the spanwise, wall-normal and time average of the velocity. The characteristic velocity is used to non-dimensionalize the velocity components. The Reynolds number based on the bulk velocity and cube height

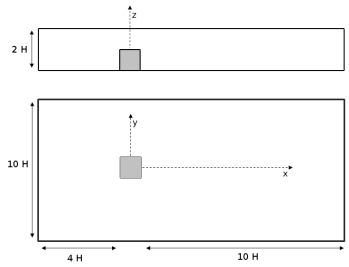

FIGURE 2.1. Geometry

(Re_H) is $Re_H = 50\,000$. A characteristic time scale (T_{ref}) can then be defined based in the velocity scale and the length scale of the cube

$$T_{ref} = \frac{H}{U_{bulk}} \approx 0.043 \text{ s}. \tag{2.2}$$

This is the time for the bulk flow to advect one length of the cube and is used to non-dimensionalize time.

2.2. Aerodynamic Train Model

The ATM is a generic train model which has 4 cars, 9 intercar gaps and simplified bogies. There are more car gaps than cars in order to model a longer train. For stability reasons, small regions between the wheels and car body, and wheels and ground are covered with *shoes* in the numerical study. This is believed to have negligible effect on the flow in the wake. The model used is scaled 1:50 to a full size train. The characteristic length of the train is the hydraulic diameter d_h. It is 3 meters in full scale, which means that $d_h = 3/50 = 0.06$ m in 1:50 scale model. The length of the train is approximately 35 d_h. The Reynolds number based on d_h and the free stream velocity U_{inf} (Re_d) is $Re_d = 60\,000$. Using the hydraulic diameter and the free stream velocity a characteristic time scale, T_{ref} can be defined as

$$T_{ref} = \frac{d_h}{U_{\text{inf}}} \approx 0.004 \text{ s} \tag{2.3}$$

which is the time for the free stream to convect one hydraulic diameter of the train and is used to non-dimensionalize time. The geometry also contains a platform and ground, which are both moving relative to the train. The computational domain extend to the walls of the water towing tank, simulating the entire flow inside the water towing tank. In the streamwise direction the domain extends half a train length in front and one train length behind the train, respectively.

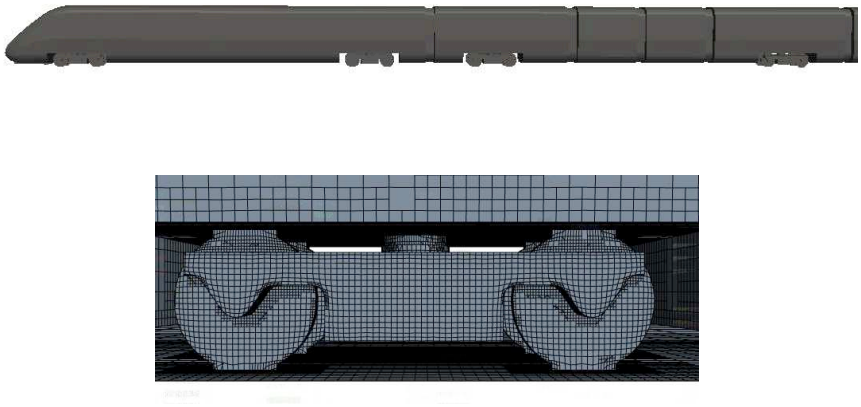

FIGURE 2.2. Geometry of train and close up on shoes at the wheels

CHAPTER 3

Turbulence modelling and Numerical Method

The simulations in this thesis were performed with the finite volume solver StarCD v4 from CD-adapco. It solves the incompressible Navier-Stokes equations,

$$\rho\frac{\partial u_i}{\partial t} + \rho u_j \frac{\partial u_i}{\partial x_j} = -\frac{\partial p}{\partial x_i} + \frac{\partial}{\partial x_j}\left(\tau_{ij}\right) \tag{3.1}$$

$$\frac{\partial u_i}{\partial x_i} = 0, \tag{3.2}$$

where τ_{ij} is the stress tensor, which for RANS based linear eddy viscosity models, for instance Spalart-Allmaras one-equation model, looks like

$$\tau_{ij} = 2\left(\mu + \mu_t\right) s_{ij} - \frac{2}{3}\left(\left(\mu + \mu_t\right)\frac{\partial u_k}{\partial x_k} + \rho k\right)\delta_{ij} \tag{3.3}$$

$$s_{ij} = \frac{1}{2}\left(\frac{\partial u_i}{\partial x_j} + \frac{\partial u_j}{\partial x_i}\right), \tag{3.4}$$

where μ_t is the turbulent viscosity, k the mean turbulent kinetic energy and the velocities are now time averaged.

In this chapter the numerical methodologies and settings used for the simulations are explained. This includes turbulence model, numerical schemes (time and space), the different computational grids and finally boundary conditions.

3.1. Detached-Eddy Simulation

Detached-Eddy Simulation (DES) is a hybrid LES/RANS type of turbulence model. The general idea is to use LES where the grid is fine enough to resolve the largest eddies and to use RANS where the grid is too coarse. The LES resolves the largest and model the smallest scales, while RANS models all the scales of turbulence. In the boundary layer LES would require very small cells and in order to save cells for DES, RANS is used close to walls and LES far from walls. The original DES formulation, later denoted DES97 was presented in Spalart *et al.* (1997). The wall distance d is replaced with a modified wall distance $\tilde{d}$, which switches between the wall distance and a filter length that depends on the cell size in the Spalart-Allmaras (SA) one-equation RANS models,

$$\tilde{d} = \min(C_{DES}\Delta, d). \tag{3.5}$$

Here C_{DES} is a constant, which is calibrated for inhomogeneous decaying turbulence to $C_{DES} = 0.65$. The other parameter Δ is related to the filter length and depends in the grid spacing in each direction,

$$\Delta = \max(\Delta x, \Delta y, \Delta z). \tag{3.6}$$

The wall distance is the replaced by $\tilde{d}$ in the destruction term in the transport equation for turbulent viscosity in the SA formulation.

$$\frac{\mathrm{D}\tilde{\nu}}{\mathrm{D}t} = c_{b1}\tilde{S}\tilde{\nu} + \frac{1}{\sigma}\left[\nabla\left((\nu+\tilde{\nu})\nabla\tilde{\nu}\right) + c_{b2}\left(\nabla\tilde{\nu}\right)^2\right] - c_{\omega 1}f_{\omega}\left(\frac{\tilde{\nu}}{\tilde{d}}\right)^2 \tag{3.7}$$

The terms of the right hand side of the equation are production, diffusion and destruction of turbulent viscosity, respectively. In regions far away from walls $\tilde{d}$ will be smaller than d. This implies, since the term is in the denominator of the destruction term, that the destruction of turbulent viscosity increase. The turbulent viscosity represent the modelled turbulence, increasing the destruction will lead to less modelled and more resolved turbulence. This is consistent with the original idea of DES.

It was later found that a poor construction of the grid could lead to a switch to LES mode also inside the boundary layer. Which could lead to too early separation, called Grid-Induced Separation (GIS). A modification to the original DES97 was proposed to remove GIS, called Delayed-DES (DDES) Spalart *et al.* (2006), where the inner part of the boundary layer is kept in RANS mode by implementing a shielding function f_d. The modified wall distance for DDES is then defined as

$$\tilde{d} = d - f_d\max(0, d - C_{DES}\Delta). \tag{3.8}$$

The shielding function is created such that it is 1 in separated regions, returning to DES97, and 0 close to walls, returning to the SA formulation ensuring RANS behaviour. This is accomplished by defining the functions as

$$f_d = 1 - \tanh\left((8r_d)^3\right), \tag{3.9}$$

$$r_d = \frac{\nu_t + \nu}{\sqrt{U_{i,j}U_{i,j}}\kappa^2 d^2}, \tag{3.10}$$

where κ is a SA constant, $U_{i,j}$ is the velocity gradients, ν_t and ν the turbulent and kinematic viscosity.

For a more comprehensive overview of DES97, DDES, other versions of DES and other hybrid LES/RANS turbulence models, we refer to Sagaut *et al.* (2006).

3.2. Discretization Methodology and Grid

The convective fluxes are discretized with the Monotone advection and reconstruction scheme (MARS) available in StarCD. It is a second order TVD scheme, which has a build in compression parameter γ. This parameter can be changed by the user between 0 and 1, where 1 yields good sharpness of the solution at the expense of slow convergence. A value of 0.9 has been chosen for most simulations performed in order to reduce the effect of smearing, but not risk a large impact of dispersion errors. MARS has been used for DES in for example Diedrichs (2009), where satisfactory results were found. The diffusive fluxes are discretized with a second order central difference scheme.

The time integration is done with the second order implicit scheme PISO, see Issa (1985). The time step is chosen such that most cells fulfill $Co < 1$ where Courant number Co is ($Co = \frac{\Delta t U}{\Delta x}$), as suggested by Spalart (2001). The timestep for the simulation on the cube is $\Delta t = 0.023\ T_{ref}$ and for the ATM $\Delta t = 0.0125\, T_{ref}$.

The trim-hexa grids used in the simulations are constructed in Star-CCM+ v3. For the surface-mounted cube different grid topologies and resolutions were tested, but the results are only presented for the grid with satisfactory results. For the ATM, results from 3 different grid (CM, MM, FM) are presented to show the grid dependence of the results. The prismlayers are the same for these 3 grids but the resolution elsewhere is changed. The difference in cell lengths between the coarsest and the finest mesh is $\sqrt{2}$ in each direction, proposed by Spalart (2001). The grid for the cube contain 12 prism layers and 3 refinements zones and the grids for the ATM 5 layers and 6 zones. A total of 4.2 million cells are used for the cube, while the corresponding amount is 11, 20 and 28 million cells for CM, MM and FM, respectively. Pictures of the grids are shown in Figure 3.1.

3.3. Boundary Conditions

There are four types of boundary condition used for the two geometries: wall, inflow, pressure outlet and symmetry. The wall boundary condition applies a no-slip condition, which means that the tangential velocity component is zero to the impermeable wall, meaning that the wall normal component is zero. The no-slip condition is imposed via a hybrid wall model, which switches between wall function and low-Re treatment depending on the y^+ value. The grids for the two geometries resolve the boundary layer to $y^+ \approx 1$, expecting low-Re treatment in most of the domain. Some of the walls are moving in the reference frame used. This means that the free stream velocity is imposed

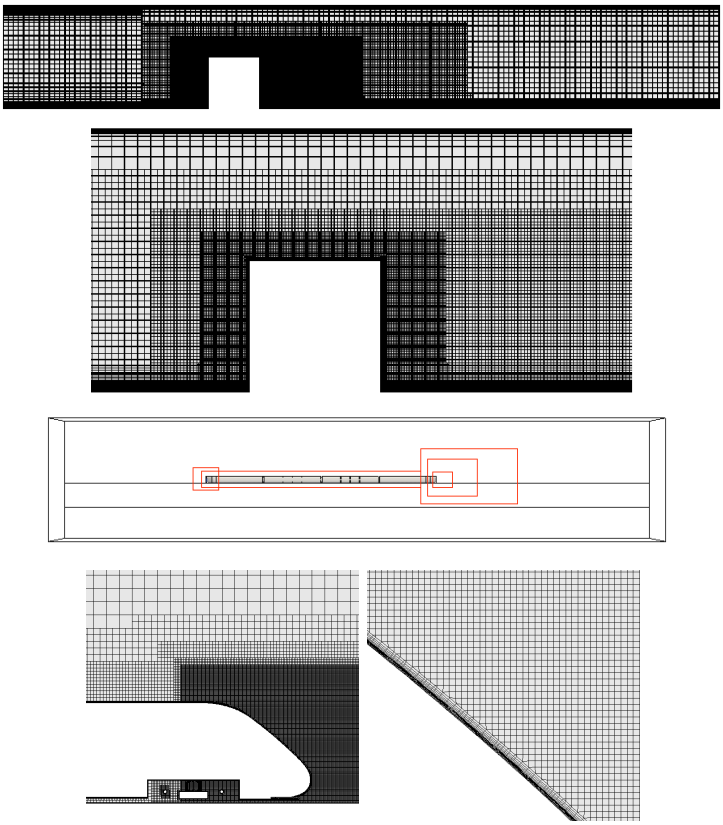

FIGURE 3.1. Grid refinement zones and grid for the cube and train

at the wall, i.e. that instead of being zero the tangential flow has a constant velocity component.

The inlet are for both geometries a Dirichlet boundary condition, perscribing all the velocity components and turbulent quantities. However, since the cube is situated inside the channel and the train model move into stationary fluid, the turbulent quantities at the inlet are different. For internal flow the turbulence intensity in the free stream is much higher, about one order of magnitude, than for external flow. The turbulence intensity (TI) for the cube is approximated to $TI = 4$ % from empirical formulas for channel pipe flow and for the ATM is estimated from the experimental results to $TI = 0.3$ %. The length scale of turbulence (L_T) for the cube is estimated using empirical formulas to $L_T = 0.14\ H$, while for the train it is estimated to $L_T = 0.1 d_h$ from Casey & Wintergerste (2000). It was found that it is important for the simulation on the cube to correctly model the turbulence at the inlet. In

order to obtain a fully converged turbulent flow as upstream input data a separate simulation is performed on a empty channel with periodic boundary conditions. Velocity cross sections of the flow is stored and used as boundary data in the simulation including the cube in the channel. For the ATM, the velocity is constantly equal to U_{inf} plus small random fluctuations across the inlet boundary.

Downstream of the obstacles a pressure outlet boundary condition is used. The pressure is set constant zero gauge over the boundary, the tangential components are specified to zero and the wall normal component is extrapolated from the domain. The symmetry boundary condition specifies that no particle can go trough the boundary, meaning that the normal velocity component is zero, and zero gradient of all other velocities across the boundary, i.e. wall normal derivative is equal to zero.

Similar type of boundary conditions are used for the simulation on both geometries. The difference is the symmetry condition that is used for the cube and the moving walls that are used for the ATM. The important difference is the the stationary walls that is applied at the channel walls, making the simulation internal, while the moving wall is applied far from the ATM making that simulation charactericed as external, eventough it is inside a water tank.

CHAPTER 4

Decomposition Methods

The flow in wakes behind bluff bodies are transient, chaotic and 3-dimensional, which means that it is difficult to analyze the full flow field directly. The purpose of decomposition methods is to separate the flow field into two parts, one that depends on time and one that depend on space. The spatial part then describes a structure in the flow that evolve in the manner that the time dependant part dictates. Instead of analyzing the flow field, the flow structures can be analyzed individually and only those structures that are important to the flow or the question of issue need to be considered. This means for instance that structures that contain low amount of energy are neglected, if energy content of the flow are of interest. The are many different decomposition methods available, each having different properties and the corresponding modes show different behaviour. The two decomposition methods used to analyze the flow around the surface-mounted cube and the ATM are POD and Koopman modes decomposition. These two methods and their properties are explained below. For both methods the velocity field is used to compute the modes, this is done in a discrete manner by saving instances in time, snapshots, of the discrete flow field. In both methods $N_T = m + 1$ snapshots of N_P grid points is stored in a matrix $\mathbf{U}$

$$\mathbf{U} = \begin{bmatrix} u(x_1,t_1) & & u(x_1,t_{N_T}) \\ v(x_1,t_1) & \cdots & v(x_1,t_{N_T}) \\ w(x_1,t_1) & & w(x_1,t_{N_T}) \\ & \ddots & \\ u(x_{N_P},t_1) & & u(x_{N_P},t_{N_T}) \\ v(x_{N_P},t_1) & \cdots & v(x_{N_P},t_{N_T}) \\ w(x_{N_P},t_1) & & w(x_{N_P},t_{N_T}) \end{bmatrix} = \begin{bmatrix} \mathbf{u}_1 & ... & \mathbf{u}_{N_T} \end{bmatrix}. \tag{4.1}$$

4.1. Proper Orthogonal Decomposition

Proper Orthogonal Decomposition was originally proposed by Lumley (1967) as a method to extract coherent structures. A detailed description of the derivation can be found in Cazemier *et al.* (1998) or Manhart & Wengle (1993). In

POD either one of two Fredholm integral equations of the second type are solved, either for the time coefficients a_i or the basis functions $\vec{\sigma_i}$

$$\lambda^n a^n(t) = \iint u_i(x_j, t')u_i(x_j, t)\mathrm{d}\Omega a^n(t')\mathrm{d}t' \tag{4.2}$$

$$\mu^n \sigma_i^n(x_k) = \iint u_i(x'_k, t)u_j(x_k, t)\mathrm{d}t\sigma_j^n(x'_k)\mathrm{d}\Omega'. \tag{4.3}$$

These equations are eigenvalue problems, and have the property that the eigenfunctions are orthogonal and that all the eigenvalues are real and positive. The two equations are dependant and hence only one of them needs to be solved. Eq. (4.2) or (4.3) are discretized, so that the integrals can be approximated by sums. It is useful to arrange the discrete values into matrices and use matrix operation to describe the sums. The size of the resulting matrices is very different depending on which of the eigenvalue problem that is chosen. Using the equation for the time coefficients leads to a eigenvalue problem of size $N_T \times N_T$, while using the other equation leads to a problem of size $3N_P \times 3N_P$. Since $N_P >> N_T$ the eigenvalue problem for the time coefficients is less demanding to solve. Arranging the time coefficients into a matrix $\mathbf{A}$ the eigenvalue problem becomes

$$\Lambda\mathbf{A} = \mathbf{C}\,\mathbf{A} \tag{4.4}$$

Here $\mathbf{C}$ is the temporal correlation matrix that only depend on the flow field and the discritization of the computed flow field. Once the time coefficients are known the basis functions can easily be calculated, by projecting the velocity field onto the time coefficients.

4.2. Koopman Mode Decomposition

Koopman mode decomposition decomposes the flow field in a different way than POD. Here the modes are separated by frequency of the motion of each flow structure. Koopman mode decomposition has only recently been introduced in fluid mechanics studies. One first study is presented in Rowley *et al.* (2009), where a jet in crossflow is analyzed using Koopman mode decomposition and POD. In that flow field two dominating flow structures were found, one far up in the jet and one close to the wall in the wake behind the jet.

To introduce the methodology, consider a discrete dynamical system

$$\mathbf{u}_{k+1} = \mathbf{f}(\mathbf{u}_k), \tag{4.5}$$

where the function $\mathbf{f}$ shifts the velocity field $\mathbf{u}_k$ from one time step to the next. The Koopman operator (U) is defined as a linear operator such that

$$Ug(\mathbf{u}_k) = g(\mathbf{f}(\mathbf{u}_k)), \tag{4.6}$$

where g is a scalar valued function. In the following, g, is called an observable, and can be any quantity of interest in the flow. The Koopman operator is

hence the operator that shifts any scalar function forward in time. We denote the eigenvalues of U by λ_i and the eigenvectors φ_i, i=1,2,... Let $\mathbf{g}$ denote any vector observable of the initial flow field $\mathbf{u}_1$. As an example $\mathbf{g}$ can be the force on an object in the flow. In Mezić (2005) it is shown that $\mathbf{g}$ can be expanded in the eigenvectors of the Koopman operator as

$$\mathbf{g}(\mathbf{u}_1) = \sum_{j=1}^{\infty} \varphi_j(\mathbf{u}_1)\mathbf{v}_j \tag{4.7}$$

where $\mathbf{v}_j$ is the j-th vector valued expansion coefficients. In a similar manner, the observables at all time instances can be expanded into the same Koopman eigenvectors as for the initial step, since

$$\mathbf{g}(\mathbf{u}_{k+1}) = U^k\mathbf{g}(\mathbf{u}_1) = U^k \sum_{j=1}^{\infty} \varphi_j(\mathbf{u}_1)\mathbf{v}_j = \sum_{j=1}^{\infty} \lambda_j^k \varphi_j(\mathbf{u}_1)\mathbf{v}_j \tag{4.8}$$

This means that the infinite velocity matrix $\mathbf{U}_\infty$, $\mathbf{U}_\infty = [\mathbf{u}_1\ \mathbf{u}_2\ ...]$, can be represented in terms of the same Koopman modes as in (34), that is

$$\mathbf{U}_\infty = \mathbf{\Phi}\mathbf{S}, \tag{4.9}$$

where

$$\mathbf{\Phi} = \begin{bmatrix} \varphi_1(\mathbf{u}_1)\mathbf{v}_1 & \varphi_2(\mathbf{u}_1)\mathbf{v}_2 & \dots \end{bmatrix} \tag{4.10}$$

and

$$\mathbf{S} = \begin{bmatrix} 1 & \lambda_1 & \lambda_1^2 & \cdots \\ 1 & \lambda_2 & \lambda_2^2 & \cdots \\ \vdots & & \vdots & \ddots \end{bmatrix}, \tag{4.11}$$

Note that $\mathbf{S}$ is a Vandermonde matrix. The eigenvalues of the Koopman operator hence describe the time development of each Koopman mode. Again, the modes can be described as characteristic flow structures. This means that the entire flow can be described by the Koopman modes and the eigenvalues of the Koopman operator.

The algorithm, also referred to as Dynamic Mode Decomposition (DMD), to compute the Koopman modes for the finite dimensional velocity matrix $\mathbf{U}$ is based the Arnoldi method presented in Ruhe (1984), which gives the basis to calculate an approximation of the modes. In the Arnoldi method the m first snapshots are used to express the next snapshot $\mathbf{u}(t_{m+1})$,

$$\mathbf{u}_{m+1} = \sum_{i=1}^{m} c_i\mathbf{u}_i + \mathbf{r} \tag{4.12}$$

where the c_i are unknown coefficients chosen such that the residual $\mathbf{r}$ is minimized in the L_2-norm. The c_i obtained are then used to build the companion

matrix $\mathbf{C}$,

$$\mathbf{C} = \begin{bmatrix} 0 & 0 & \cdots & 0 & c_1 \\ 1 & 0 & \cdots & 0 & c_2 \\ 0 & 1 & \cdots & 0 & c_3 \\ \vdots & & \ddots & & \vdots \\ 0 & 0 & \cdots & 1 & c_m \end{bmatrix}. \tag{4.13}$$

In this way the computed flow field can be related to the next time step via

$$\begin{bmatrix} \mathbf{u}_2 & \mathbf{u}_3 & ... & \mathbf{u}_{m+1} \end{bmatrix} = \begin{bmatrix} \mathbf{u}_1 & \mathbf{u}_2 & ... & \mathbf{u}_m \end{bmatrix} \cdot \mathbf{C} + \mathbf{r}\mathbf{e}^T, \tag{4.14}$$

where $\mathbf{e} = (0, ..., 0, 1)$ is zero except for the m-th component.

Next the eigenvalues, $\tilde{\lambda}_i$, and eigenvectors, $\tilde{\mathbf{T}}$, of $\mathbf{C}$ are derived, where the eigenvalues of $\mathbf{C}$ are called the Ritz values. In Rowley *et al.* (2009) it is shown that $\tilde{\lambda}_i$ are approximations to the eigenvalues of the Koopman operator. That is, the eigenvalues of the companion matrix $\mathbf{C}$ are closely related to the Koopman modes as follows. First the eigenvectors of $\mathbf{C}$ are known to span the inverse of the finite Vandermonde matrix $\tilde{\mathbf{S}}$, Chen & Louck (1996),

$$\tilde{\mathbf{S}} = \begin{bmatrix} 1 & \lambda_1 & \lambda_1^2 & \cdots & \lambda_1^m \\ 1 & \lambda_2 & \lambda_2^2 & \cdots & \lambda_2^m \\ \vdots & & \vdots & \ddots & \vdots \\ 1 & \lambda_m & \cdots & & \lambda_m^m \end{bmatrix}. \tag{4.15}$$

Recall that the infinite Vandermonde matrix, $\mathbf{S}$, is used in the expansion into the Koopman eigenvectors in Eq. (4.9). Writing in a similar manner as Eq. (4.9)

$$\mathbf{U} = \tilde{\mathbf{\Phi}}\tilde{\mathbf{T}}^{-1} \tag{4.16}$$

$$\mathbf{g}(\mathbf{u}_k) = \sum_{i=1}^{m} \tilde{\lambda}_i^k \tilde{\boldsymbol{\phi}}_i \quad 1 \leqslant k \leqslant m. \tag{4.17}$$

Eq. 4.17 can be identified as the finite version of Eq. (4.8) with $\tilde{\boldsymbol{\phi}}_i = \varphi_i(\mathbf{u}_1)\mathbf{v}_i$. This means that $\tilde{\mathbf{\Phi}}$ contains the Koopman modes to the finite dimensional problem and can be calculated as

$$\tilde{\mathbf{\Phi}} = \mathbf{U} \cdot \tilde{\mathbf{T}}. \tag{4.18}$$

In order to arrange the modes it is useful to define the global energy norm of the Koopman modes,

$$\| \tilde{\boldsymbol{\phi}}_j \| = \sum_{i=1}^{N_P} \tilde{\boldsymbol{\phi}}_{i,j} \tilde{\boldsymbol{\phi}}_{i,j} w_i, \tag{4.19}$$

where the index i represtent the grid point i, j the velocity component and w_i is the volume of each cell respectively. This sum is a discrete approximation to the integral over the volume of decomposition.

The eigenvalues of $\mathbf{C}$ determine the growth rate and frequency of each mode. In order to get the frequencies, ω_i, of the each Koopman mode, the eigenvalues λ_i associated with the time discrete problem Eq. (4.5) have to be related to the eigenvalues, Γ_i, of the time continuous problem, $\dot{\mathbf{u}}(t) = \mathbf{f}(\mathbf{u}(t))$, since the eigenvalues λ_i is obtained from the Koopman mode decomposition. The frequencies can be written in terms of λ_i as

$$\omega_i = \mathrm{Im}(\Gamma_i) = \arctan\left(\frac{\mathrm{Re}(\lambda_i)}{\mathrm{Im}(\lambda_i)}\right)/\Delta t. \tag{4.20}$$

where Δt the time step between the snapshots. For more see Bagheri *et al.* (2009).

CHAPTER 5

Results and Discussion

This chapter summarizes the results obtained both on the surface-mounted cube and the Aerodynamic Train Model. These are two very different flows, but the underlaying assumption is that the decomposition methods introduced in Section 4 can be used for both cases. First the flow field are compared to available data. This is important since if the input data is invalid, the analyzing tool can not extract the correct coherent structures. The results computed is then decomposed into POD and Koopman modes. The modes are then analyzed with the aim to obtain an improved understanding of the flow field and to identify characteristic flow structures. One part is dedicated to compare the two decomposition methods.

5.1. Flow Field

For the surface-mounted cube the available data is rich and many different studies can be used for comparison. Especially useful is Rodi *et al.* (1997), in which different LES simulations are compared, which gives an understanding of the spread in results for different studies. Also, it is valuable to compare with experimental data as those presented in Martinuzzi & Tropea (1993). The most important comparison is with the results in Manhart & Wengle (1993), where also POD modes are calculated. This comparison between flow fields gives an approximation of how large difference between the POD modes that can be expected. The comparison is shown in Figure 5.1.

The results are satisfactory since the DES computations fall within the spread of the LES computation for the mean velocity field. The mean Reynolds stress value on top of the cube show a underestimation for the DES computations, but only one numerical simulation is available for comparison and therefore the spread of results is not known. In the wake the level of mean Reynolds stress is similar between the three different studies, but the profiles are different. The fluctuations in the wake simulated with DES is therefore considered to be adequate to extract the dominant flow structures.

For the ATM the only available data for comparison are the water tunnel experiments. During the course of the numerical investigation it was found that the model in the experiments was equipped with a trip wire. This results were found to be very difficult to replicate and therefore no comparison is

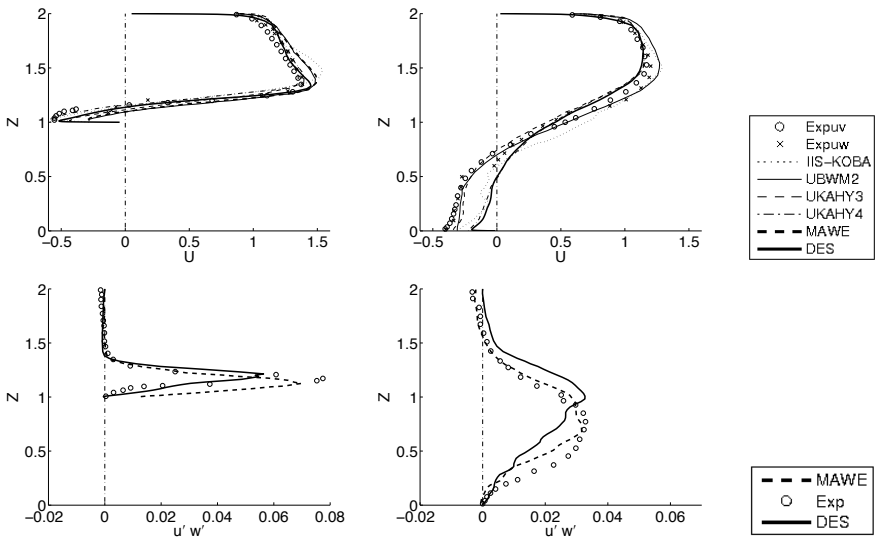

FIGURE 5.1. Velocity profiles

presented. Instead different numerical grids were tested in order to prove grid independent results. Velocity profiles in different regions of the flow between the coarse, medium and fine mesh are compared in Figure 5.2 and 5.3. Figure 5.2 show the results along the side of the train and Figure 5.3 shows the results in the wake of the train.

The results show that there is only a small difference between the fine and medium mesh at certain part of the flow. While the coarse mesh deviates quite far from the other grids at a few key positions. The coarse is therefore deemed inadequate, but the results of the medium grid is considered satisfactory.

The results on both the surface-mounted cube and the ATM are considered to simulate the main features of the flow and it is therefore expected that the decomposition will reveal the dominating flow structures.

5.2. Mode Decomposition

A selection of the decomposed modes are presented in this section for the two different geometries. These are selected in order to illustrate different kinds of typical behaviour of the modes.

5.2.1. *Surface-mounted cube*

The first three POD modes of the flow around the surface-mounted cube is shown in Figure 5.4. These three show different behaviour and each representing a group of modes with similar behaviour. The first group is simply the

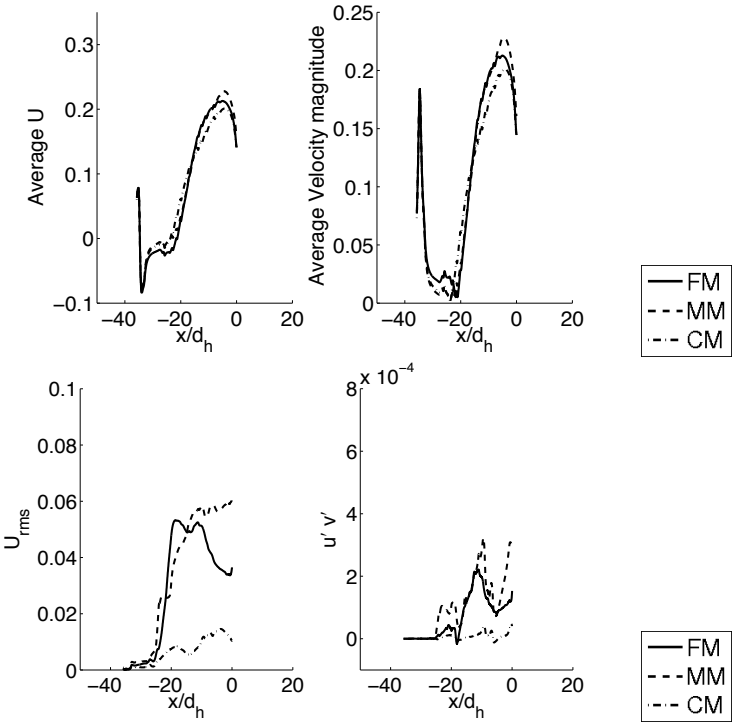

FIGURE 5.2. Mean velocity and u_{rms} on the side of the train with different grids

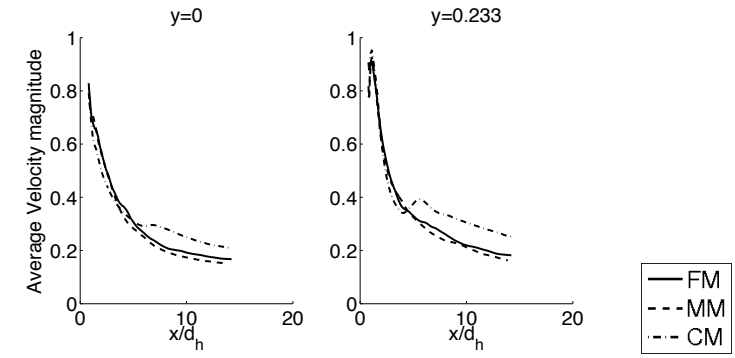

FIGURE 5.3. Mean velocity in the wake of the train with different grids as a function of streamwise position

mean flow. This is a characteristic of POD that the mean flow is extracted in the first mode. The second mode and group contains the horseshoe vortex in front of the cube and also the shear layer at the edge of the wake. This group

is therefore related to the shear layer interaction between the free stream and the disturbed flow. The third mode and group represent the flow structures inside the wake within the large separated region. The Koopman modes 1,2,9 are presented in Figure 5.5, and they show exactly the same type of groups and behaviour.

5.2.2. *Aerodynamic Train Model*

A selection of POD modes of the flow in the wake of the ATM is shown in Figure 5.6. It shows POD mode 1,2,4. What is found for the ATM is that there is a strong pairing of successive modes. Mode 2 is strongly linked to 3 and 4 to 5 and so on. This would suggest the propagation of a flow structure downstream in the wake. The two modes interact to move the structure downstream. This is also found when investigating the convergence of the modes. The first mode is as for the surface-mounted cube the mean flow and the rest involve the counter rotating vortices in the wake. It is clear that mode 2 contain a structure of larger scale in space than mode 4, which means that larger structures contain more energy.

Similar structures as in the POD modes are found in the Koopman modes, they are also dominated by the counter rotating vortices. Koopman modes 1,3 and 5 is shown in Figure 5.7. One interesting structure can be found in Koopman mode 3 in the v-component. Close to the train body two isolated structures appear that seem to be curved over the sides of the train. Recalling the explanation of the origin of the counter rotating vortices in Morel (1980), that the flow is forced into the wake over the side edge and rolls into the vortices. This structure seem to be associated with this phenomenon. Traces of this structure can be seen in other modes and also for POD, but it is only for this Koopman mode the structure is clear.

5.3. Comparing Decomposition Methods

Even though the two different decomposition methods show similar type of behaviour, they have differences. The difference is clear when investigating the frequencies of each mode. The Koopman modes are associated with one frequency each, while POD modes have no such property. The spectrum of POD modes 2,3 compared to the full spectrum of all the Koopman modes for the surface-mounted cube are shown in Figure 5.8. The POD modes have a broadband signal superpositing different frequencies (Koopman modes). From the spectrum it is also clear why there exist different group of flow structures. One group is clustered at low frequencies and the other at medium frequency. The POD mode 2 excite low frequency which is consistent with the fact that it show similar behaviour as Koopman modes in this region. The corresponding statement for mode 3 is also true for the medium frequency. The amplitudes in the spectrum is normalized with the maximum amplitude for that spectrum,

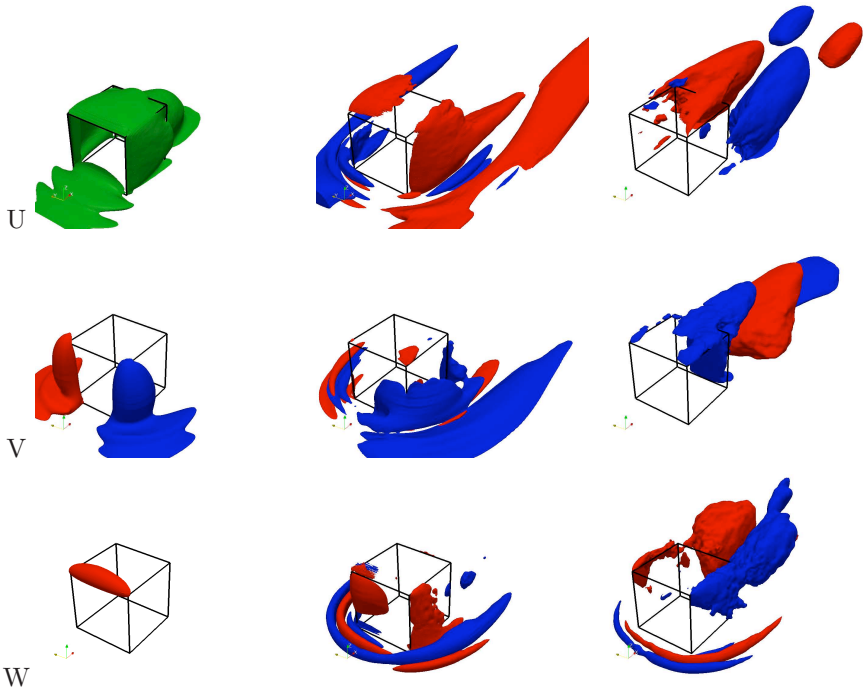

FIGURE 5.4. POD modes 1-4

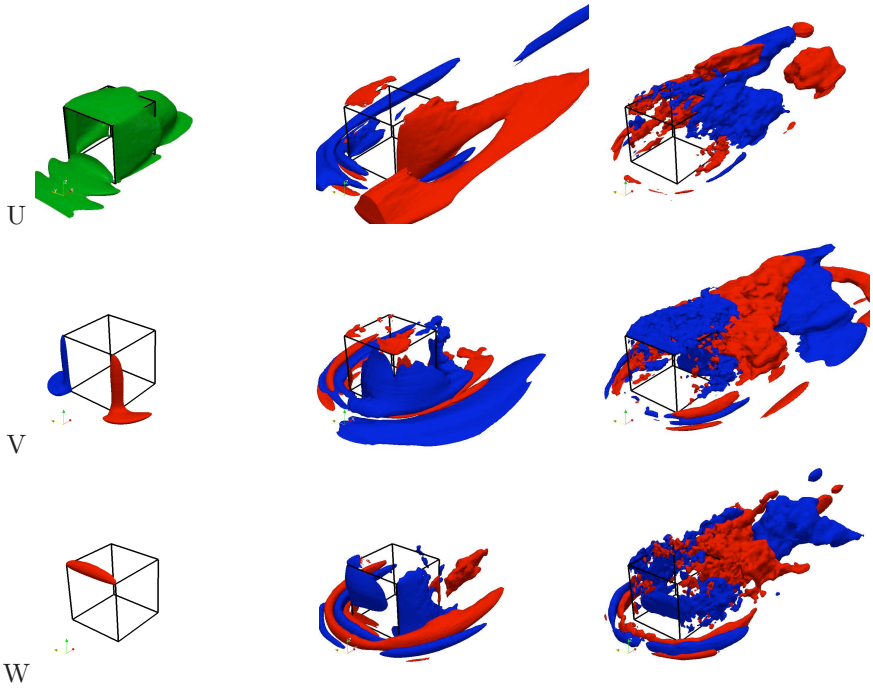

FIGURE 5.5. Koopman modes 1,2,9

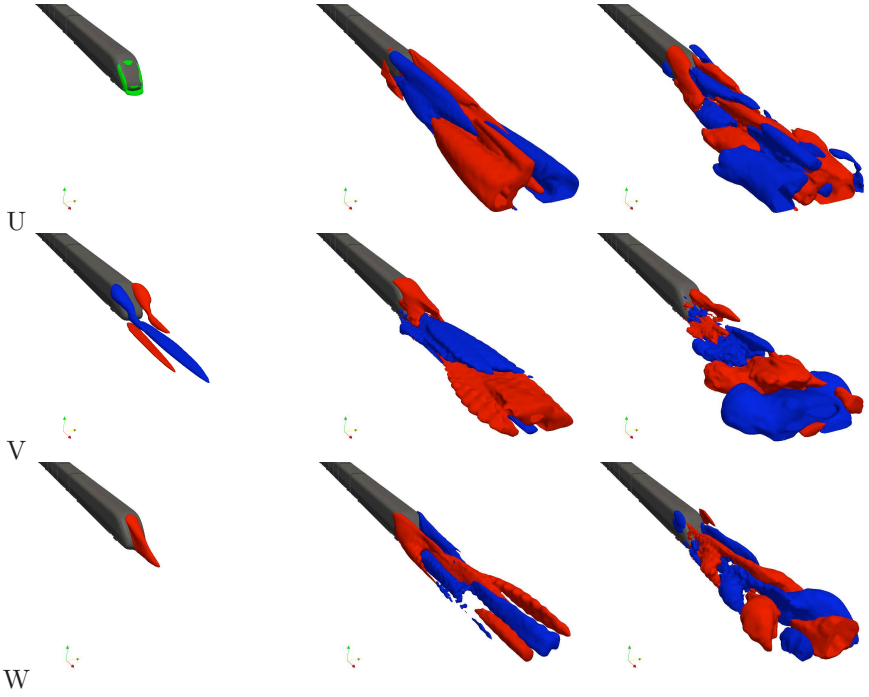

FIGURE 5.6. Isosurfaces of spatial POD modes 1,2,4

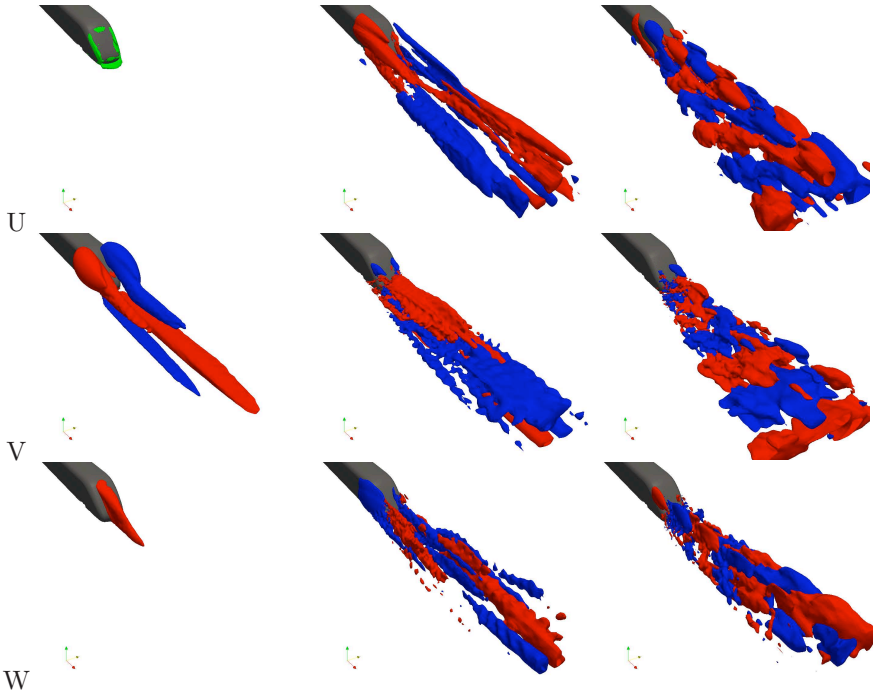

FIGURE 5.7. Isosurfaces of spatial POD modes 1,3,5

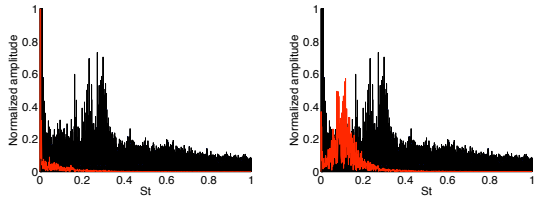

FIGURE 5.8. Spectrum of POD mode 2 (left) and 3 (right) (in red) compared to all the frequencies of Koopman (in black) for the surface-mounted cube. Each spectrum is normalized by its highest frequency.

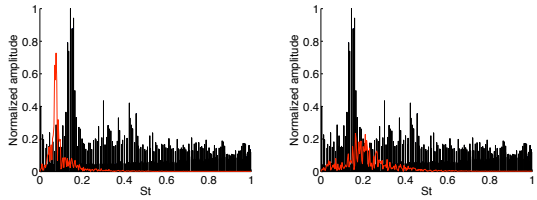

FIGURE 5.9. Spectrum of POD mode 2 (left) and 4 (right) (in red) compared to all the frequencies of Koopman (in black) for ATM. Each spectrum is normalized by its highest frequency.

which means that the computed amplitudes can not be compared between methods.

For the ATM the spectrum of the Koopman modes compared to the frequency of 2 fluctuating POD modes are shown in Figure 5.9. This shows that second and third POD modes have very similar frequency spectrum with a peak around St=0.08. The fourth mode has a higher frequency, which is consistent with the smaller spatial scales that appear in the basis functions. The Koopman modes around St=0.15 is the most dominant in the Koopman spectrum. The spectrum for the ATM has much more destinct dominant frequencies, while the cube has a more broad range of frequencies. This has to do with the fact that the ATM is external flow and the cube in internal.

5.4. Analyzing Flow Structures

It is clear from the analysis and the mode decomposition that the two geometries used in the thesis have very different wake topology. This is not unexpected since the geometries are very different and have very different ambient conditions. What is interesting is that the two different topologies seems to be the once that Morel (1980) and others have found, separation bubble and two counter rotating vortices. It is therefore important to compare the different flow structures in the different topologies and see the differences and if any similarities exist. The surface-mounted cube has a separation

bubble and 3 different types of flow structures are found, mean flow, shear layer and flow inside the separation bubble. These groups can be distinguished by looking at the basis functions or analyzing frequency of the time coefficients.

The flow behind the ATM is dominated by the other type of flow topology, which means that the modes are also dominated by the two counter rotating vortices. The difference between the modes then becomes the spatial length scales of the flow structures. The largest structures contain the most energy and need less amount of snapshots to converge compared to higher order modes.

The advantage of Koopman modes is that each structure oscillate with one frequency, which is believed to contain more information on the origin of the structure. On the other hand POD extract the large dominant structure which contain the most energy, which could also be desirable. When looking at the basis functions both of the methods extract similar structures, which show strength of both methods.

CHAPTER 6

Conclusion and Outlook

For slipstream the most important region of the flow is the near wake, where the flow is complicated with many different time and space scales. To analyze this complicated flow, mode decomposition can be used to extract coherent flow structures. The simulated flow field with DES has proven adequate to use for decomposition into POD and Koopman modes. The modes have been investigated for two different geometries, surface-mounted cube and the ATM, which exhibit very different flow topologies in the wake. The resulting modes extract the most dominant structures of each topology. Around the surface-mounted cube the flow is characterised with a separation bubble and three groups of flow structures were found. First the mean flow and then two type of perturbations around this mean, which are relating to the shear layer and the propagation of vortices inside the wake respectively. For the ATM the flow is dominated by two counter rotating vortices behind the train and these are also dominating the fluctuating modes. The POD modes and Koopman modes show similar behaviour of flow structures, with the difference that POD modes excite different frequencies while the Koopman modes isolate each frequency.

Further research would be aimed at understanding the origin of the different wake topologies and which topology that would reduce slipstream effects. More train geometries will also be analyzed in order to understand how slipstream could be improved on trains in traffic. Since the current methods are computationally demanding, attempt of increasing efficiency by reducing the simulated domain should be investigated.

CHAPTER 7

Summary of Papers

Paper 1

Mode Decomposition on a Surface-Mounted Cube.
In this paper mode decomposition of flow computed with DES is investigated. The surface-mounted cube was chosen as a test case, since various data exist to be used for comparison and validation. The comparison was done with both experimental and numerical work obtained by LES simulations. The results compared well to the different studies and it was therefore found that the DES simulation contained the relevant dominant flow structures. The flow field could therefore be used to decompose into POD and Koopman modes. In order to have reliable results two different techniques of investigating convergence of the POD modes are proposed and tested. It was found that long sample times are needed and that the two method gives consistent results. The converged modes are analyzed and three different groups of flow structures were characterized. The first group is simply the mean flow and the two others represent perturbations to this mean flow. They are dominant in different regions of the flow, the first represent perturbations at the shear layer and and the second perturbations in the wake of the cube. These flow structures would be representative of the flow topology of the wake, which is a separation bubble.

Paper 2

Detached Eddy Simulation and Validation on the Aerodynamic Train Model.
This paper compares the results obtained on the Aerodynamic Train Model with Detached Eddy Simulation and experimental work performed in a water towing tank, where the velocity field was measured using Particle Image Velocimetry. A problem of matching the streamwise position of experimental data compared to the numerical study is discovered. This is solved by identifying the position of the head pressure pulse for both methods and using this position in order to calibrate the position. Promising results are found when comparing the mean and rms velocities in the wake of the high-speed train model. However, the results when comparing the results alongside the train body shows discrepancies, which at this point could not be explained. The flow field was also analyzed with the Q-criterion and two counter-rotating vortices in the wake of the train is identified.

Paper 3

Mode Decomposition of the Flow Behind the Aerodynamic Train Model Simulated by Detached Eddy Simulation.

The flow around the ATM was investigated further in order to understand the discrepancies between the experiments and the numerical simulations. It was found that the difference originated from a trip wire that was present in the experimental work. An attempt to model the effect of the trip wire was done, but it was not found possible to duplicate the experimental results, with this approach. A grid dependence study was performed and a mesh with 20 million cells was found adequate to use. The analyzing methodology using mode decomposition that was previously tested on the the surface-mounted cube was used on the ATM, including the convergence investigation. The flow topology of the ATM is very different from that of the surface-mounted cube and therefore different flow structures were extracted. The flow structures of the ATM is solely related to the two counter rotating vortices in the wake. These vortices are very dominant structures and contain most of the energy in the wake. The largest structures contain the most energy and converge faster than higher order modes.

Acknowledgements

First I would like to thank my two supervisors Prof. Dan Henningson and Associate Prof. Gunilla Efraimsson for helping me to make this thesis by creating a interesting, joyful, challenging and supportive research environment. I have enjoyed working for you.

The work would not have been possible without the close collaboration with Bombardier Transportation, where I would like to thank Dr. Astrid Herbst for the collaboration, exchange of knowledge and data, contacts made and project leadership. Also Dr. Alexander Orellano's comments and knowledge exchange is deeply appreciated.

This work has been financed by Banverket through the Gröna Tåget research program, which is gratefully acknowledged.

The experimental work used for comparison was performed at the German Aerospace Centre (DLR). The exchange of data and information has been vital to this work, and I appreciate all the efforts made by Mattias Jönsson and Prof. Andreas Dillmann. Prof. Dillmann and Prof. Thomas Rung are also acknowledged for being part of the reference group for this project, which has contributed with a lot of good feedback during the course of the work.

Important when doing numerical simulations are to have large and good computational resources. This has been made available at PDC and NSC through Swedish National Infrastructure for Computing (SNIC), all involved parties are acknowledge.

I would also like to extend my gratitude to the lunch/fika group consisting of Ciarán, Dmitry, Jia, Sathish, Tristan and others who have come and left. I enjoy our lunch traditions, eventhough we usually have problems deciding where to go. And would also like to thank all the people at both AVE and MECH, too many to mention everyone. Being involved in two departments can sometimes be difficult but with the help of many nice people I have always seen it as an advantage and opportunity. A thank you to Malte for being my contact within the Mechanics department.

Last I would like to thank my father and brother for always supporting me in my (academic) life and also for the family field trip to Monaco to study Vehicle Aerodynamics of Motorsport.

Bibliography

Ahmed, S., Ramm, G. & Faltin, G. 1984 Some Salient Features Of The Time-Averaged Ground Vehicle Wake. *SAE-Paper 840300*.

Alfonsi, G., Restano, C. & Primavera, L. 2003 Coherent structures of the flow around the surface-mounted cubic obstacle in turbulent channel flow. *Journal of Wind Engineering and Industrial Aerodynamics* **91**, 495–511.

Andersson, E. & Berg, M. 2007 *Spårtrafiksystem och spårfordon*. Stockholm.

Bagheri, S., Åkervik, E., Brandt, L. & Henningson, D. 2009 Matrix-Free Methods for the Stability and Control of Boundary Layers On the Identification of a Vortex. *AIAA Journal* **47**, 1057–1068.

Baker, C. 2001 Flow and dispersion in ground vehicle wakes. *Journal of Fluids and Structures* **15**, 1031–1060.

Barrot, J. 2008 Commission Decision of 21 february 2008 concerning a technical specification for interoperability relating to the rolling stock sub-system of the trans-European high-speed rail system. *Official Journal of the European Union* **L84(51)**.

Bergmann, M., Cordier, L. & Brancher, J.-P. 2005 Optimal rotary control of the cylinder wake using POD Reduced Order Model. *Physics of Fluids* **17(9)**, 097101:1–097101:21.

Bocciolone, M., Cheli, F., Corradi, R., Muggiasca, S. & Tomasini, G. 2008 Crosswind action on rail vehicles: Wind tunnel experimental analyses. *Journal of Wind Engineering and Industrial Aerodynamics* **96**, 584–610.

Casey, M. & Wintergerste, T. 2000 (Eds.) ERCOFTAC Special Interest Group on Quality and Trust in Industrial CFD Best Practice Guidelines. *ERCOTFTAC*.

Cazemier, W., Verstappen, R. & Veldman, A. 1998 Proper orthogonal decomposition and low-dimensional models for driven cavity flows. *Physics of Fluids* **10(7)**.

CD-adapco 2008 STAR-CD Version 4.06 Documentations.

Chen, W. & Louck, J. 1996 The combinatorial power of the companion matrix. *Linear Algebra and its Applications* pp. 261–278.

Chevalier, M., Schlatter, P., Lundbladh, A. & Henningson, D. 2007 Simson-A Pseudo-Spectral Solver for Incompressible Boundary Layer Flows. *Technical Report KTH Mechanics*.

Diedrichs, B. 2009 Unsteady Aerodynamic Crosswind Stability of a High-Speed

Train Subjected to Gusts of Various Rates. *Proceedings Euromech Colloquium 509: Vehicle Aerodynamics* pp. 39–50.

Favre, T. 2009 Numerical Investigation of Unsteady Crosswind Aerodynamics for Ground Vehicles. *Licentiate Thesis*.

Figura-Hardy, G. 2007 RSSB Slipstream Safety - Analysis of existing experimental data on train slipstreams including the effects on pushchairs. *Rail Safety and Standards Board*.

Hamida, H., Krajnović, S. & Davidson, L. 2005 Large-Eddy Simulation of the Flow Around a Simplified High Speed Train Under the Influence of a Cross-Wind. *Proceedings of the* 17^{th} *AIAA Computational Fluid Dynamics Conference*.

Issa, R. 1985 Solution of the Implicitly Discretised Fluid Flow Equations by Operator-Splitting. *Journal of Computational Physics* **62**, 40–65.

Jeong, J. & Hussain, F. 1995 On the Identification of a Vortex. *Journal of Fluid Mechanics* **285**, 69–94.

Jönsson, M., Haff, J., Richard, H., Loose, S. & Orellano, A. 2009 PIV Investigation of the Flow Field underneath a Generic High-Speed Train Configuration. *Proceedings Euromech Colloquium 509: Vehicle Aerodynamics* pp. 119–130.

Kee, J., Kim, M. & Lee, B. 2001 The COANDA FLOW control and Newtonian concept approach to achieving drag reduction of a passenger vehicle. *SAE Paper 2001-01-1267*.

Krischer, K., Rico-Martinez, R., Kevrekidis, J., Rotenmund, H., Ertl, G. & Hudson, J. 1993 Model identification of a spatiotemporal varying catalytic reaction. *American Institute of Chemical Engineers Journal* pp. 89–98.

Lumley, J. 1967 The structure of inhomogeneous turbulent flows. *In Atmospheric Turbulence and Radio Wave propagation (A.M. Yaglom and V.I. Tatarsky, eds.)* pp. 166–178.

Manhart, M. & Wengle, H. 1993 A Spatiotemporal Decomposition of a Fully Inhomogeneous Turbulent Flow Field. *Theoretical and Computational Fluid Dynamics* **5**, 223–242.

Martinuzzi, R. & Tropea, C. 1993 The Flow around a Surface Mounted Prismatic Obstacle Placed in a Fully Developed Channel Flow. *ASME Journal of Fluids Engineering* **115**, 85–92.

Menter, F. & Kuntz, M. 2004 Adaptation of Eddy-Viscosity Turbulence Models to Unsteady Separated Flow Behind Vehicles. *In: R. McCallen, F. Browand and F. Ross. Symposium on the Aerodynamics of Heavy Vehicles: Trucks, Buses and Trains*.

Mezić, I. 2005 Spectral properties of dynamical systems, model reduction and decompositions. *Nonlinear Dynamics* **41**, 309–325.

Morel, T. 1980 Effect of base slant on flow in the near wake of an axisymmetric cylinder. *Aeronautical Quarterly* **31**, 132–147.

Muld, T., Efraimsson, G. & Henningson, D. 2010 Mode decomposition on surface mounted cube. *Submitted to Flow, Turbulence and Combustion*.

Muld, T., Efraimsson, G., Henningson, D., Herbst, A. & Orellano, A. 2009 Detached eddy simulation and validation on the Aerodynamic Train Model. *Proceedings Euromech Colloquium 509: Vehicle Aerodynamics* pp. 174–187.

Rodi, W., Ferziger, J., Breuer, M. & Pourquié, M. 1997 Status of Large Eddy Simulation: Results of a Workshop. *Journal of Fluids Engineering* **119**, 248–262.

Rowley, C., Mezić, I., Bagheri, S., Schlatter, P. & Henningson, D. 2009 Spectral analysis of nonlinear flows. *Journal of Fluid Mechanics* **641**, 115–127.

Ruhe, A. 1984 Rational Krylov sequence methods for eigenvalue computations. *Linear Algebra and its Applications* **58**, 391–405.

Rung, T. 1999 Formulierung universeller Wandrandbedingungen für Transportgleichungsturbulenzmodelle. *Institutsbericht Nr. 02/99, Hermann-Föttinger-Institut für Strömungsmechanik, Technische Universität Berlin*.

Sagaut, P., Deck, S. & Terracol, M. 2006 *Multiscale and Multisolution Approaches in Turbulence*. Imperial college press, Singapore.

Schober, M., Orellano, A., Cheli, F., Rocchi, D. & Tomasini, G. 2009 Comparison of the wind tunnel test results on the ATM train. *Proceedings Euromech Colloquium 509: Vehicle Aerodynamics* pp. 211–222.

Spalart, P. 2001 Young-person's guide to Detached-Eddy Simulation grids. *NASA CR 2001-211032*.

Spalart, P., Deck, S., Shur, M., Squires, K., Strelets, M. & Travin, A. 2006 A new version of detached-eddy simulation, resistant to ambiguous grid densities. *Theoretical and Computational Fluid Dynamics* **20**, 181–195.

Spalart, P., Jou, W.-H., Strelets, M. & Allmaras, S. 1997 Comments on the feasibility of LES for wings, and on a hybrid RANS/LES approach. *First AFOSR International Conference on DNS/LES*.

Sterling, M., Baker, C., Jordan, S. & Johnson, T. 2008 A study of the slipstreams of high-speed passenger trains and freight trains. *Proceedings of the Institution of Mechanical Engineers, Part F: Journal of Rail and Rapid Transit* **222**, 177–193.

Travin, A., Shur, M., Strelets, M. & Spalart, P. 1999 Detached-Eddy Simulations past a circular cylinder. *Flow, Turbulence and Combustion* **63**, 293–313.

Travin, A., Shur, M., Strelets, M. & Spalart, P. 2002 Physical and numerical upgrades in the Detached-eddy simulation of complex turbulent flows. *In: R. Friedrich and W. Rodi. Advances in LES of Complex Flows*.

Turk, M. & Pentland, A. 1991 Face recognition using eigenfaces. *Proceedings of 1991 IEEE Computer Society Conference on Computer Vision Pattern Recognition* pp. 132–147.

Weller, J., Lombardi, E., Bergmann, M. & Iollo, A. 2009 Numerical methods for low-order modeling of fluid flows based on POD. *International Journal for Numerical Methods in Fluids*.

Yang, Z., Johnson, J., Morley, J., Unaune, S. & Sovani, S. 2007 Dynamic moving mesh CFD study of semi-truck passing a stationary vehicle with hood open. *SAE Paper 2007-01-0111*.